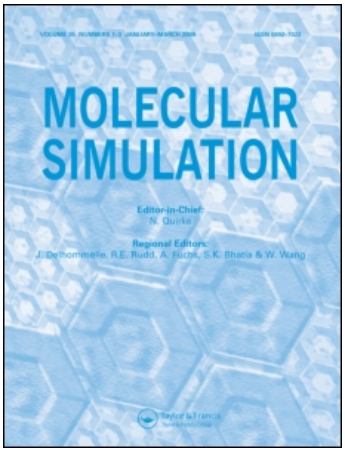


**Molecular Simulation**
Publication details, including instructions for authors and subscription information:
http://www.informaworld.com/smpp/title~content=t713644482

# Nanofluidics: Molecularly thin lubricant layers under confinement

T. Becker[a]; F. Mugele[a]
[a] Department of Applied Physics, University of Ulm, Ulm, Germany

**To cite this Article** Becker, T. and Mugele, F.(2005) 'Nanofluidics: Molecularly thin lubricant layers under confinement', Molecular Simulation, 31: 6, 489 — 494
**To link to this Article: DOI:** 10.1080/08927020412331337069
**URL:** http://dx.doi.org/10.1080/08927020412331337069

*Molecular Simulation*, Vol. 31, Nos. 6–7, 15 May – 30 May 2005, 489–494



# Nanofluidics: Molecularly thin lubricant layers under confinement

T. BECKER* and F. MUGELE

Department of Applied Physics, University of Ulm, Albert Einstein Allee 11, 89069 Ulm, Germany

*(Received November 2004; in final form December 2004)*

Confined liquid films with a thickness in the range of a few molecular diameters exhibit different mechanical properties than in the bulk. With the technique of a 2-dimensional (2D) imaging surface forces apparatus (SFA) we investigated in detail the layer by layer thinning of a thin liquid film confined between two atomically smooth surfaces upon pressing them towards each other with increasing load. The dynamics of a series of subsequent squeeze-out processes of individual layers were analyzed. Using a simple hydrodynamic model, we extracted the thickness-dependence of the viscosity. For the system investigated here—the model lubricant Octamethylcyclotetrasiloxane (OMCTS) confined between ultraclean, recleaved mica surfaces—we found that the viscosity increased by a factor of 10 with decreasing the film thickness from 6 to 2 layers. We decomposed the friction into two components, one describing the sliding of liquid layers on top of the substrates, and the other describing liquid-on-liquid sliding. The latter contribution was found to agree closely with expectations based on the bulk viscosity, whereas the former was approximately 35 times higher for the present system.

*Keywords*: Surface forces apparatus; Octamethylcyclotetrasiloxane; Confined liquid films; Microelectromechanical systems; Elasto-hydrodynamics; Nanotribology



## 1. Introduction

The ongoing progress in science and technology concerning micro- and nanosystems poses new questions about the materials used in this regime. In particular, liquids exhibit a completely different behavior when they are confined to the molecular range [1]. Liquid films with a thickness in the molecular range find application in microelectromechanical systems (MEMS) where they act as lubricant and protect devices from excessive wear. Here, the stability of the liquid film is of crucial importance. But also in conventional applications like lubrication in modern car engines one is interested in the stability of such molecularly thin lubricant layers in order to reduce fuel consumption. To reduce the friction and improve the lifetime of the engine it is necessary to know the behavior of the lubricating liquid in this confined geometry in detail.

We first consider the model situation of two atomically smooth and homogenous plates at a variable separation with a liquid in between. Here, one can observe the following behavior. The molecules in the vicinity of the rigid walls arrange into layers parallel to the confining walls, which is already well established in the literature [2–7]. This gives rise to density oscillations extending a few molecular diameters from each surface into the bulk. Applying an external normal force on the plates results initially in a continuous decrease of the gap width. At a certain separation, the oscillatory density profiles emanating from the confining walls begin to overlap. At this point, drainage ceases to be a continuous process. Instead, it occurs in a step-like fashion where each step corresponds to the squeeze out of one molecular layer. In order to squeeze out a liquid layer, the normal force on the surfaces has to exceed a certain threshold value, which increases with decreasing thickness. This behavior is sometimes referred to as layering transitions. In conventional surface forces apparatus (SFA) experiments the force between the confining surfaces is measured as a function of the film thickness [3–6]. Measuring the force as a function of separation results in an oscillatory function. The force varies between attraction and repulsion and the periodicity of the oscillation correlates well with the size of the molecules. In contrast to these measurements, we do not measure forces. Here, we will analyze the dynamics of the layering transitions using the recently developed 2-dimensional (2D) imaging technique for the SFA [8]. We will briefly outline the principles of

*Corresponding author. E-mail: thomas.becker@physik.uni-ulm.de

*Molecular Simulation*
ISSN 0892-7022 print/ISSN 1029-0435 online © 2005 Taylor & Francis Group Ltd
http://www.tandf.co.uk/journals
DOI: 10.1080/08927020412331337069

this technique. Then we will describe experimental results and their interpretation with respect to confinement-induced viscosity enhancement. As we will show, the resolution of the imaging technique with respect to viscosity is much higher than that of conventional shear force measurements. Most of the experiments described here were already described in [9–11]. A predominantly theoretical review of squeeze processes of thin lubricant layers was given in [12].

## 2. Experiment and sample preparation

The measurement of the thickness of the liquid films is a crucial for any SFA experiments. The standard procedure in SFA experiments is the so called fringes of equal chromatic order (FECO)-technique [13–15]. The samples are illuminated with white light, which produces interference fringes, when light passes through a multi-layer system composed of silver mirrors, two mica substrates, and the liquid film. The wavelength of the transmitted fringes is analyzed with a spectrometer. Two atomically smooth and ultra-clean mica-sheets with an evaporated silver layer of typically 45 nm thickness on their backside are glued onto a curved sample support. The samples are mounted in a crossed cylinder geometry and thus form a Fabry–Perot Interferometer with adjustable gap width. For the 2D imaging technique used in the present experiment, we illuminate the samples from below with monochromatic light [8,9,22]. The wavelength is adjusted to the wing of one of the transmission peaks of the interferometer. The transmission through this multi-layer system is recorded with a CCD-camera equipped with a microscope objective. When the surfaces are brought into contact, elastic flattening of the mica samples gives rise to a roughly circular contact area with an homogeneous distance between the silver mirrors is formed. This can clearly be seen in the homogeneous gray level of the contact area in the 2d-transmission images (see figure 1). Furthermore, due to the sample geometry Newton rings around the contact can be seen. When the thickness of the liquid changes at a given location within the contact area, this gives rise to a different gray level (see figure 1). Quantitative information about the thickness changes is obtained using the so-called fast spectral correlation (FSC) developed by Heuberger and coworkers [16] based the matrix method [17] for optical multilayers. The thickness resolution thus obtained is of the order of 0.2 nm.

The preparation of the mica substrates is of crucial importance for viscosity measurements. Small defects and inhomogeneities on the mica surfaces can affect the behavior of the adjacent liquid in the molecular range. The standard substrate preparation procedure that had been in use for many years [3,5–7,18] was shown recently to produce nanometer sized contamination particles, which have a strong influence on friction force measurements [19–21]. We used a modified surface preparation procedure that avoids this type of contamination [10,11,22].

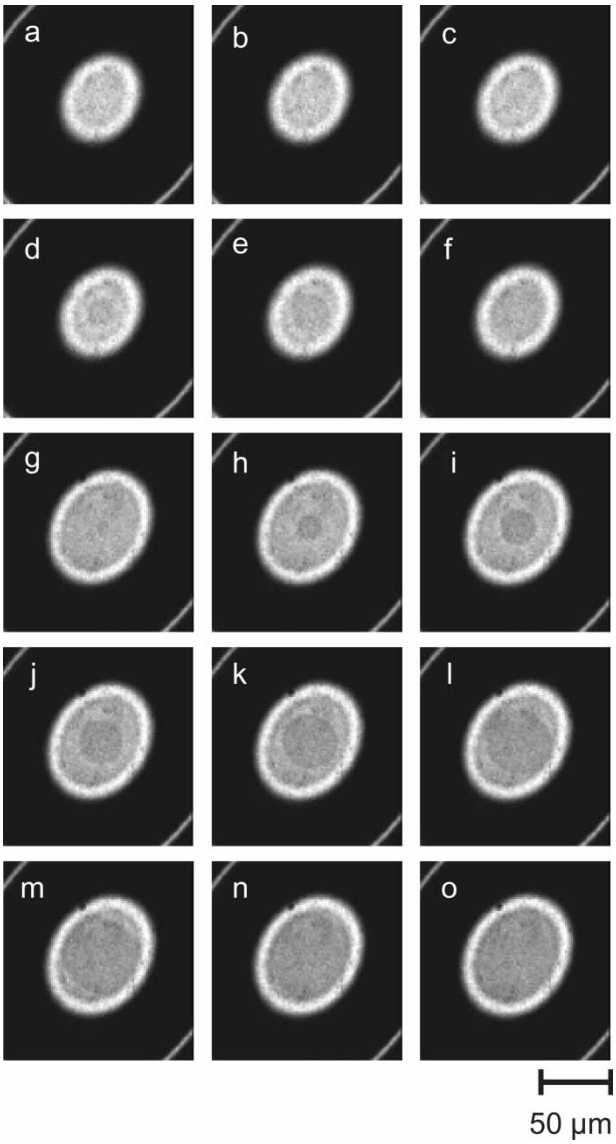


Figure 1. Series of snapshots from two subsequent layering transitions. For images a–f: $\Delta t = 50$ ms, for images g–o: $\Delta t = 100$ ms. Due to the substrate elasticity, the contact area grows with increasing load. Darker gray level in the contact area corresponds to thinner liquid film thickness. The velocity of the boundary line in the first layering transition (images a–f) is approximately three times larger than in the following layering transition (images g–o).

Once the samples are prepared and installed, liquid is injected into the cell. The experiments presented here were performed with Octamethylcyclotetrasiloxane (OMCTS), a non-polar silicone-oil with quasi-spherical molecules. More precisely the molecules are an oblate spheroids with major diameter of 1.0–1.1 nm and minor diameter of 0.7–0.8 nm [3]. Additionally, a container with $P_2O_5$ as drying agent is placed into the cell to ensure dry conditions. After injecting the liquid into the cell, the surfaces are brought into contact with each other and after several minutes a liquid neck forms at the edge of the contact area due to capillary condensation [23].

The experiments were performed at a room temperature of (22 ± 1)°C.

After a certain time of equilibration at a surface separation of several microns the surfaces are pressed together. Figure 1 shows images from a video sequence of an experimental run with a continues increasing load ramp pressing the surfaces together. It can be clearly seen that the increase of the external force results in an elastic flattening of the contact area. Usually, the diameter of the contact area is approximately 50–100 μm. From time to time (figure 1d and h) darker areas appear within the contact area and subsequently spread over the contact area. A smaller value of transmission corresponds to decreased film thickness, because the wavelength of the incident monochromatic light was adjusted to the right side of a transmission peak. Figure 2 shows the transmitted intensity averaged over an area of 5 × 5 $\mu m^2$ within the contact region as a function of time. One can clearly distinguish four different steps in intensity. In between these step, the value of transmission remains more or less constant. To determine the change in thickness between these steps, the matrix method is used again [9,17]. The steps in intensity of the experimental data shown in figure 2 correspond to (0.8 ± 0.1) nm, which is in agreement with the diameter of the OMCTS molecules. We thus can use this technique to observe layering transitions in real time, in particular the dynamics of single layers of OMCTS confined between two mica surfaces.

We now analyze the growth rate of the areas with reduced film thickness. The nucleation and the growth of the island with a reduced one molecular layer thickness ($n - 1$) can be described as follows. The applied normal force on the surfaces exerts a pressure on the liquid layers. Due to thermal fluctuations, a hole in a liquid layer nucleates. The elastic relaxation of the mica into this hole transforms the external 3-dimensional pressure into a 2D driving force, which pushes the liquid layer towards the edge of the contact area. Against this driving force acts the friction of the liquid with respect to the substrate. The dynamics of the layering transitions can be understood in terms of a simple hydrodynamic model developed by Persson and Tosatti [1,24]. Here, an incompressible 2D fluid is assumed. The basic equations of this model are the continuity equation and a generalized Navier–Stokes equation for a two dimensional velocity field $v(x,t)$:

$$\frac{\partial}{\partial t} v + v \cdot \nabla v = \frac{1}{\rho_{2D}} \nabla p + \upsilon \nabla^2 v - \eta_{\text{eff}} v \qquad (1)$$

In this expression, $\nu$ is the kinematic viscosity and $p$ is the 2D pressure. Neglecting the nonlinear and the viscosity terms and assuming a slowly changing velocity field, that the time derivative can be neglected, one obtains the following equation:

$$\nabla p = -\rho_{2D} \eta_{\text{eff}} v \qquad (2)$$

Thus, the dynamics are governed by the balance between the driving force due to the 2D pressure gradient within the contact area and the dissipative drag force term. The drag force term on the right side of the equation consist of the 2D density $\rho_{2D}$, an effective friction coefficient $\eta_{\text{eff}}$ and the velocity $v$ of the boundary line between the regions of different film thickness. The accessible quantity in the experiments is the velocity of the boundary line of the layering transitions. We extract the radius of the area of film thickness ($n - 1$) from the video images and plot it vs. the time (see data points in figure 3). The slope of the curves represents the velocity of the boundary line. The plot clearly shows, that speed of the boundary line decreases with decreasing film thickness. Experimental data are fitted using an analytical solution of the equation above with a single fitting parameter, namely the effective friction coefficient $\eta_{\text{eff}}$. Indeed, the investigation of the effective frictional coefficient $\eta_{\text{eff}}$ shows, that $\eta_{\text{eff}}$ increases with decreasing number of liquid

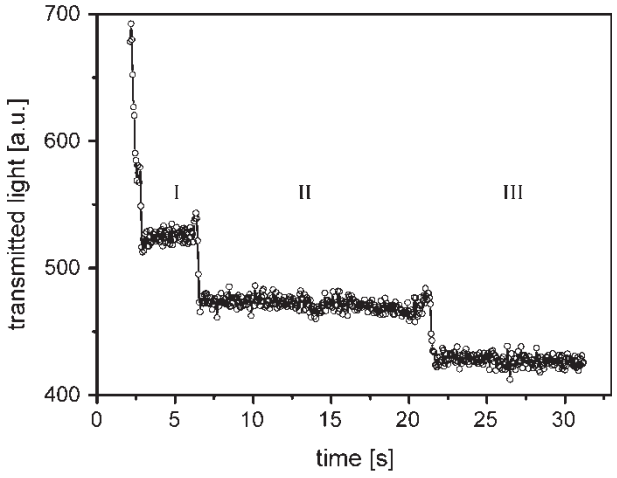


Figure 2. Transmitted intensity averaged over an area of 5*5 $\mu m^2$ within the contact area during an external load ramp. The plateaus correspond to steps in thickness of (0.8 ± 0.1) nm of the liquid film due to the layering transitions.

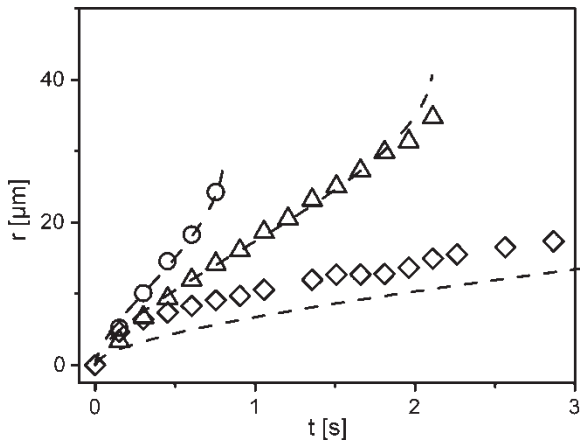


Figure 3. Radius of the island with reduced film thickness ($n - 1$) vs. time for three subsequent layering transitions (circles: $n = 5 \rightarrow 4$, triangles: $n = 4 \rightarrow 3$, squares: $n = 3 \rightarrow 2$). The lines correspond to the theoretical fits of the model by Persson and Tosatti. The decreasing slope of the curves results in an increasing effective friction coefficient $\eta_{\text{eff}}$.

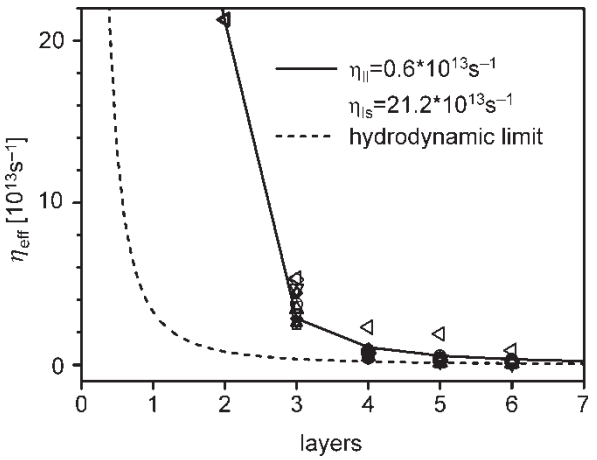


Figure 4. Effective friction coefficient vs. number of molecular layers of OMCTS taken from different experimental runs. The solid line represents the best fit calculation using the extended Persson–Tosatti model. For larger film thickness, the effective friction coefficient converges to the flow resistance calculated in the hydrodynamic limit (dashed line).

layers (figure 4). Reducing the number of layers from 6 to 2 results in an increase of the friction coefficient by somewhat more than one order of magnitude.

This result is in contrast with experiments in the past, where the mica-samples were prepared in the standard procedure [6,7,18,25], which claimed a much stronger increase. For some of these experiments, it is now clear that the discrepancy is due to contamination problems in the earlier measurements [20,21].

To understand the increase of the viscosity, we consider the layering transitions on a microscopic level (see figure 5). During a layering transition, the contact area is composed of three different regions. In the region ahead of the moving boundary line, the liquid molecules adopt a well defined layer structure with $n$ layers. In the (second) region, around the boundary line, the liquid is expected to be rather disordered, whereas in the third region—behind the moving boundary line—the layer structure is again well pronounced, but now with a thickness of only $(n - 1)$ layers. Due to mass conservation the material ahead of the boundary line moves towards the edge of the contact area. Frictional processes involved in this motion give rise to dissipation. For a mathematical description, we extend the hydrodynamic model by

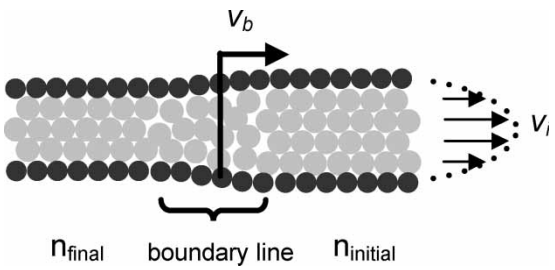


Figure 5. Microscopic model for the liquid layer expulsion process $n = 4 \rightarrow 3$. Due to limited optical resolution the boundary regime in the recorded images appears as a sharp line.

Persson–Tosatti to a multilayer system. We include a coupling between adjacent layers by analogous viscous drag terms and assume the 2D pressure $p_{2D}$ to be distributed evenly between all layers [10]. Furthermore, we introduce two different friction coefficients. The first, the liquid–liquid friction coefficient $\eta_{ll}$, arises from the sliding of two adjacent liquid layers on top of each other. The top and the bottom layers interact on one side with other liquid molecules and on the other side with the solid wall. This liquid–solid friction is taken into account with the coefficient $\eta_{ls}$. The set of equations can be solved and one obtains as expected a parabolic velocity profile for the liquid layers between the confining mica [10].

The experimentally observed quantity is the velocity of the boundary line, which is due to mass conservation given by the sum of the velocities of the single layers:

$$v_b = \sum_{i=1}^{n} v_i \tag{3}$$

We can now fit the experimentally observed behavior in figure 4 using the two friction coefficients as fitting parameters (solid line in figure 4). We find reasonable agreement with the experimental data for friction coefficients of $\eta_{ls} = 21.2 \times 10^{13}\,s^{-1}$ and $\eta_{ll} = 0.6 \times 10^{13}\,s^{-1}$, respectively. The agreement with the experimental data suggests that our assumption of a thickness-independent value of $\eta_{ll}$ is justified. Since the latter does not depend on the film thickness $n$, the effective friction coefficient $\eta_{eff}$ should converge for large film thickness $n \rightarrow \infty$ vs. the flow resistance of a thin film calculated in the hydrodynamic limit, which is given by:

$$\eta(d) = \frac{12\eta_{bulk}}{\rho d^2} \tag{4}$$

The value $\eta_{ll-hydro} = 0.3 \times 10^{13}\,s^{-1}$ calculated in the hydrodynamic limit is reasonably close to the best fit value for $\eta_{ll}$. The sliding between adjacent layers of ordered liquid thus gives rise to a momentum transfer that is rather close to the situation for a completely disordered bulk liquid. The reason for the increase of the experimental data compared to the extrapolated bulk behavior (dashed line in figure 4) is the increasing weight of $\eta_{ls}$ compared to $\eta_{ll}$ for decreasing $n$.

The results described so far refer to a system with relatively hard (thick) mica substrates. If we repeat the same experiment for a system with softer (i.e. thinner) mica sheets and increase the load rate in addition, elastohydrodynamic effects change the scenario of squeeze out. Figure 6a shows some images from a video with soft substrates and a high approach rate [26]. The nucleation of the liquid layer occurs at several places at the edge of the contact area and most of the liquid is trapped in the contact area. This liquid patch shrinks with time and forms a droplet, which is expelled out of the contact region within the next few seconds. Bringing the surfaces together very quickly the liquid exerts an additional pressure on the mica surfaces due to its finite viscosity.

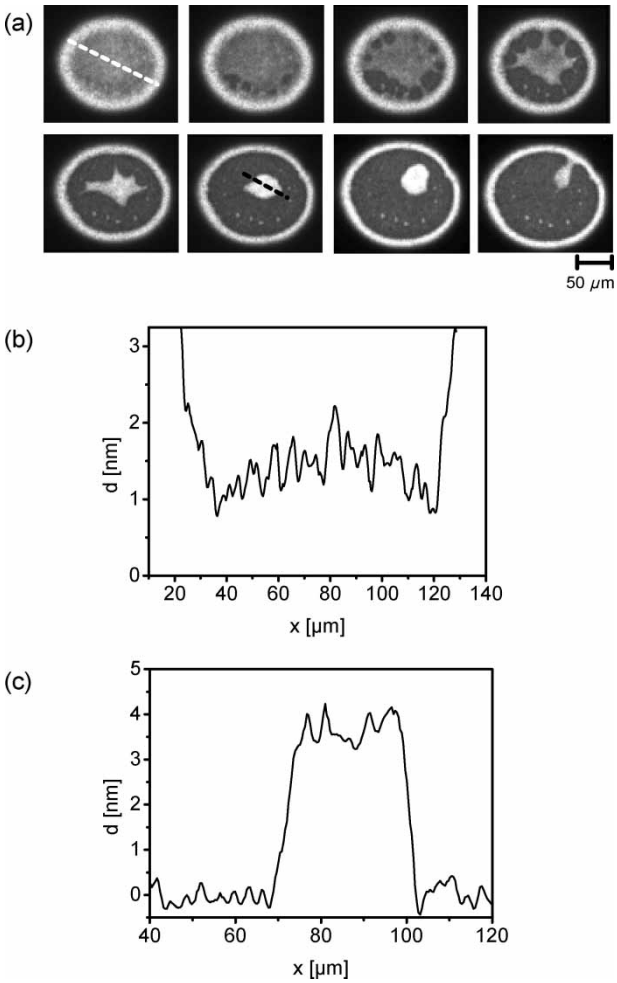


Figure 6. Snapshots of an experimental run with a load-ramp applied to soft substrates. (a) The liquid film nucleates at several places at the edges of the contact area. Darker gray corresponds to thinner film thickness. The trapped liquid shrinks to a droplet with time and is pushed out of the contact area by a resulting force due to the pressure distribution in the contact area. (b) The reason for nucleation at the edge of the contact area is given by the thickness distribution of the liquid due to elastohydrodynamic deformation of the substrate (height profile in the first image). The height profile in (c) shows the shape of the trapped droplet with a film thickness of (3.7 ± 0.1)nm, which corresponds to four discrete layers of OMCTS molecules.

This leads to an outward bending of the mica and can be clearly seen in the profile across the image in the beginning of the approach (figure 6b). Now the separation between the solid substrates is much smaller at the edge of the contact area and the liquid film nucleates at several places. Due to the elastic relaxation of the mica the trapped liquid shrinks and forms a droplet. It is remarkable, that this droplet has very sharp edges and a flat top, as shown in the height profile in figure 6c. The height of the droplet is (3.7 ± 0.1) nm, which corresponds to four layers of OMCTS. The expulsion of this drop can be understood as follows. The pressure inside the contact area is governed by a pressure distribution with a maximum in the center of the contact area, for example a Hertzian pressure distribution. The drop is placed a little bit off-centered and thus on each point of the boundary

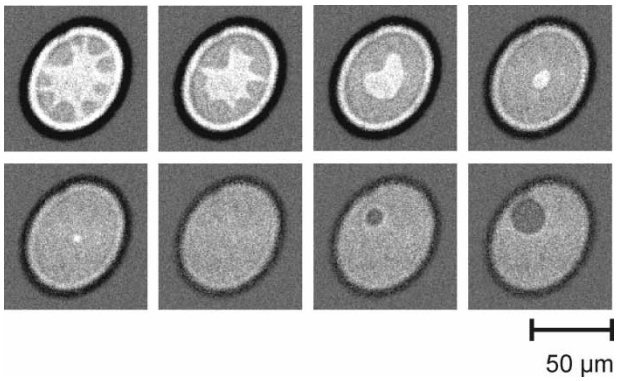


Figure 7. Mixed scenario of layering transitions between stiff mica substrates with a high surface approach rate. Whereas in the beginning the layering transitions nucleate at several places at the edge of the contact area and the liquid is pushed into neighbored layers, the last recorded layering transition ($n = 3 \rightarrow 2$) spreads towards the edge of the contact area.

acts a different pressure. Integrating along the boundary of the drop yields a resulting force directed to the edge of the contact area, which drives the droplet out of the contact region [12]. From the dynamics of this expulsion we determined a value for the effective friction coefficient of $\eta_{\text{eff}} = 2.4 \times 10^{13}\,\text{s}^{-1}$, which is in the same order of magnitude as with the thick substrates.

Depending on the stiffness of the substrates and on the speed of the load ramp, we may also find a mixed scenario (figure 7). In the beginning of the approach it can be clearly seen, that the liquid film nucleates at several points at the edge of the contact area. The trapped liquid patch shrinks and the bright area, which corresponds to the larger film thickness, vanishes in the center of the contact area. In contrast to the thin substrates no trapped droplet is formed, but the liquid molecules is pushed into adjacent layers and then squeezed out of the contact area (see figure 8). So what we found again is the elastohydrodynamic behavior of the system in the beginning, where the mica surfaces are bent outwards due to the additional pressure exerted by the liquid. Once the mica surfaces have relaxed, the expulsion behavior changes to the situation with the nucleation close to the center of the contact area and the last liquid layer observed in this experimental run spreads to the edge of

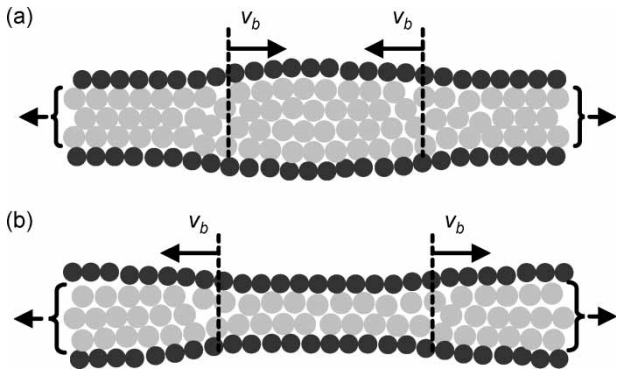


Figure 8. Schematic sketch of the layering transition $n = 4 \rightarrow 3$ (a) and $n = 3 \rightarrow 2$ (b) for stiff substrates with high applied load rate.

the contact region. Figure 7 shows the layering transitions from $n = 4 \rightarrow 3$ and from $n = 3 \rightarrow 2$ layers. During the transition $n = 4 \rightarrow 3$ (first line of figure 7) the boundary line between $n = 4$ and $n = 3$ moves inwards, as sketched in figure 8a. The subsequent transition $n = 3 \rightarrow 2$ layer nucleates close to the center of the contact area and the boundary line moves towards the edge of the contact area. In both cases, the dissipation takes place in the region between the moving boundary line and the edge of the contact area, i.e. in a region with $n = 3$ layer. A more detailed analysis of this dynamical behavior will be presented in the future.

Apart from the measurements of the effective friction coefficient in the first experiment described in this report, a close inspection of the images of the layering transitions reveals more interesting details on the boundary line dynamics. The area with reduced film thickness $(n - 1)$ is not simply circular, but it shows edges and facets (see figure 1i–k) [26]. Extracting the boundary line from the images allows a detailed analysis. We determined the orientation of short segments between adjacent pixels of the boundary line along the circumference of the island. Indeed it was found, that the facets of the boundary line occur in orientations under a preferred angle of approximately 60° between adjacent facets. It is very tempting to attribute this observation to the symmetry of the mica substrates. Indeed, recent Monte Carlo simulations of static OMCTS layers confined between mica surface showed, that the liquid adopts the pseudo-hexagonal structure of the mica lattice [27,28]. The observed effect is expected to be very sensitive to the alignment of the mica samples with respect to each other.



## 3. Conclusion

We presented our investigations on molecularly thin lubricant layers with a 2D-imaging SFA, which allows a detailed analysis of the dynamics of the layering transitions. It was shown, that the increase of the effective friction coefficient with decreasing film thickness is due to the increasing weight of the friction between the liquid molecules and the substrate compared to the liquid–liquid friction. Different behavior was observed for the layering transitions depending on substrate elasticity and surface approach rate. The cleanliness of the mica surfaces is of crucial important for all these results and was achieved with recleaving the mica substrates immediately prior to the experiment.

## Acknowledgements

We would like to thank S. Herminghaus, B. Persson, S. Granick and J. Klein for fruitful discussions and comments. We acknowledge financial support by the German Science Foundation under grant number Mu 1472/2-1 within the priority program “Wetting and Structure Formation at Interfaces”.

## References

[1] B.N.J. Persson. *Sliding Friction—Physical Principles and Applications*, Springer Verlag, Berlin (2000).
[2] J.N. Israelachvili. *Intermolecular and Surface Forces*, Academic Press, London (1991).
[3] R.G. Horn, J.N. Israelachvili. Direct measurement of structural forces between two surfaces in a nonpolar liquid. *J. Chem. Phys.*, **75**, 1400–1412 (1981).
[4] H.K. Christenson, C.E. Blom. Solvation forces and phase separation of water in a thin film of nonpolar liquid between mica surfaces. *J. Chem. Phys.*, **86**, 419–423 (1987).
[5] D.Y.C. Chan, R.G. Horn. The drainage of thin films between solid surfaces. *J. Chem. Phys.*, **83**, 5311–5324 (1985).
[6] J. Klein, E. Kumacheva. Confinement-induced phase transitions in simple liquids. *Science*, **269**, 816–819 (1995).
[7] A.L. Demirel, S. Granick. Glasslike transition of a confined simple fluid. *Phys. Rev. Lett.*, **77**, 2261–2264 (1996).
[8] F. Mugele, M. Salmeron. Dynamics of layering transitions in confined liquids. *Phys. Rev. Lett.*, **84**, 5796 (2000).
[9] F. Mugele, T. Becker, A. Klingner, M. Salmeron. Two-dimensional observation of drainage and layering transitions in confined liquids. *Coll. Surf. A*, **206**, 105–113 (2002).
[10] T. Becker, F. Mugele. Nanofluidics: viscous dissipation in layered liquid films. *Phys. Rev. Lett.*, **91**, 166104-1–166104-4 (2003).
[11] T. Becker, and F. Mugele, Mechanical properties of molecularly thin lubricant layers: experimental methods and procedures, *J. Phys. Cond. Matt.* (in press)
[12] B.N.J. Persson, F. Mugele. Squeeze-out and wear: fundamental principles and applications. *J. Phys. Cond. Matt.*, **16**, R295–R355 (2004).
[13] J.N. Israelachvili. Optical studies of thin films. *J. Coll. Int. Sci.*, **44**, 259–272 (1973).
[14] M. Ruths, S. Steinberg, J.N. Israelachvili. Effects of confinement and shear on the properties of thin films of thermotropic liquid crystal. *Langmuir*, **12**, 6637–6650 (1996).
[15] M. Heuberger, G. Luengo, J.N. Israelachvili. Topographic Information from multiple beam interferometry in the surface forces apparatus. *Langmuir*, **13**, 3839–3848 (1997).
[16] M. Heuberger. The extended surface forces apparatus. Part I. Fast spectral correlation interferometry. *Rev. Sci. Instr.*, **72**, 1700–1707 (2001).
[17] M. Born, E. Wolf. *Principles of Optics*, 6th ed., Cambridge University Press, (1999).
[18] J. Klein, E. Kumacheva. Simple liquids confined to molecularly thin layers. I. Confinement -induced liquid-to-solid phase transitions. *J. Chem. Phys.*, **108**, 6996–7009 (1998).
[19] S. Ohnishi, M. Hato, K. Zamada, H.K. Christenson. Presence of particles on melt-cut mica sheets. *Langmuir*, **15**, 3312–3316 (1999).
[20] Y. Zhu, S. Granick. Reassessment of solidification in fluids confined between mica sheets. *Langmuir*, **19**, 8148–8151 (2003).
[21] M. Heuberger, M. Zäch. Nanofluidics: structural forces, density anomalies, and the pivotal role of nanoparticles. *Langmuir*, **19**, 1943–1947 (2003).
[22] P. Frantz, M. Salmeron. Preparation of mica surfaces for enhanced resolution and cleanliness in the surface forces apparatus. *Tribol. Lett.*, **5**, 151–153 (1998).
[23] M.M. Kohonen, N. Maeda, H.K. Christenson. Kinetics of capillary condensation in a nanoscale pore. *Phys. Rev. Lett.*, **82**, 4667–4670 (1999).
[24] B.N.J. Persson, E. Tosatti. Layering transition in molecular thin films: Nucleation and growth. *Phys. Rev. B*, **50**, 5590–5599 (1994).
[25] A. Mukhopadhyay, J. Zhao, S.C. Bae, S. Granick. Contrasting friction and diffusion in molecularly thin confined films. *Phys. Rev. Lett.*, **89**, 136103-1–136103-4 (2002).
[26] T. Becker, F. Mugele. Collapse of molecularly thin lubricant layers between elastic substrates. *J. Phys. Condens. Matt.*, **15**, 321–330 (2003).
[27] J.E. Curry. Structure of a model lubricant in a mica slit pore. *J. Chem. Phys.*, **113**, 2400–2406 (2000).
[28] J.E. Curry. The mica slit-pore as a tool to control the orientation and distortion of simple liquid monolayers. *Mol. Phys.*, **99**, 745–752 (2001).